JCTC Journal of Chemical Theory and Computation

pubs.acs.org/JCTC Article

Stabilizing Leaflet Asymmetry under Differential Stress in a Highly Coarse-Grained Lipid Membrane Model

Samuel Foley and Markus Deserno*

Cite This: *J. Chem. Theory Comput.* 2020, 16, 7195−7206 Read Online

ACCESS | Metrics & More | Article Recommendations | Supporting Information

ABSTRACT: We present a version of the coarse-grained Cooke lipid model, modified to simulate asymmetric lipid membranes. It is inspired by a method employed by Wang et al. [*Commun. Comput. Phys.* **2013**, *13*, 1093−1106] for artificially penalizing lipid flip-flop but copes more robustly with differential stress, at the cost of one additional bead per lipid and the concomitant increase in computational overhead. Bilayer asymmetry ultimately breaks down beyond a system size dependent critical differential stress, which can be predicted from a simple analytical model. We remeasure many important material parameters for the new model and find it to be consistent with typical fluid lipid membranes. Maintaining a stable stress asymmetry has many applications, and we give two examples: (*i*) connecting monolayer stress to lipid number asymmetry in order to directly measure the monolayer area modulus and (*ii*) finding its strain-dependent higher-order correction by monitoring the equilibrium bilayer area.

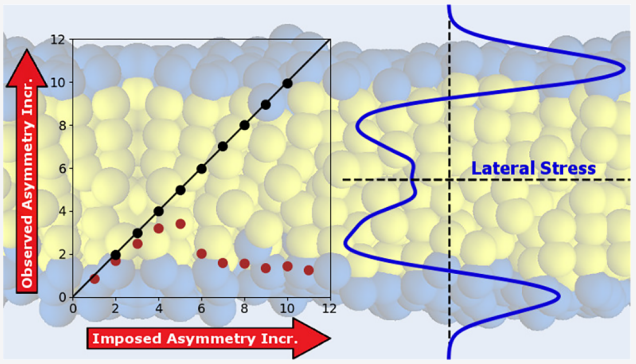

1. INTRODUCTION

1.1. Motivation. In many situations of biological interest, the lipid bilayers that form the structural basis of biomembranes feature an asymmetric distribution of lipids across their leaflets.[1−4] For instance, much of the phosphatidylcholine and most of the sphingomyelin content of the plasma membrane of nucleated cells can be found in the outer leaflet, while the majority of phosphatidylethanolamine and especially phosphatidylserine resides in the inner one.[3] This situation is remarkable, because such an asymmetric distribution is not in thermal equilibrium:[5] upon being prepared in some asymmetric state, a lipid bilayer will generally decay toward a symmetric one, in which the lipid species are mixed across both leaflets, because this maximizes entropy and equilibrates the lipids' chemical potential between leaflets. The dynamical process for achieving this compositional relaxation happens via many individual events, whimsically termed lipid "flip-flop": the transbilayer motion by which individual lipids move through the center of the bilayer to transition to the opposite leaflet. As this process perturbs local lipid order and temporarily forces the transitioning lipid's hydrophilic headgroup deep into the membrane's hydrophobic core, lipid flip-flop is associated with a sizable free energy barrier that strongly depends on lipid type.[6] Indeed, the time scale over which this process takes place tends to be fairly long compared to many other membrane-related processes (such as remodeling, fission, or fusion). The precise rate constants again vary by lipid species and context but are often on the order of hours in biologically relevant systems.[7]

Of course, cells live longer than hours. Maintaining their asymmetric membrane composition therefore requires active processes that work against the thermal driving forces toward a symmetric equilibrium. Conversely, cells may also require a local relaxation of lipid asymmetry on time scales much shorter than what thermodynamics has to offer, for instance because phospholipid synthesis mostly occurs in the cytoplasmic leaflet of the endoplasmic reticulum,[8] which hence requires a translocation of almost half of all lipids toward the other leaflet. Indeed, cells have evolved a dedicated machinery for exercising control over the trans-leaflet lipid distribution: ATP-dependent (i.e., energy consuming) flippases and floppases, which are transmembrane proteins that transport lipids (even against a gradient of chemical potential), and passive lipid scramblases, which are transmembrane proteins that catalyze lipid translocation but do not bias its directionality.[5,8]

This quick overview shall suffice to argue that cells make a significant effort to create and maintain their membranes in a precisely calibrated asymmetric state. While clearly linked to a variety of biochemical needs, this also affects more basic questions, such as the phase behavior or elasticity of such

Received: August 19, 2020
Published: October 30, 2020

https://dx.doi.org/10.1021/acs.jctc.0c00862
J. Chem. Theory Comput. 2020, 16, 7195−7206

asymmetric bilayers. However, probing these issues by performing experiments on actual biomembranes in cells, or patches excised out of cells, proves to be a coin with two sides: while clearly being as realistic as it gets, the intricacy of the real situation (complex lipid mixtures, embedded and adsorbed proteins, connections to the cytoskeleton, *etc.*) makes it almost impossible to analyze and explain the data using quantitative predictive models, thus rendering measurements less clear-cut than one would otherwise hope. Thankfully, recent breakthroughs[9−16] in the preparation of asymmetric model membranes with controllable leaflet composition have opened up a middle road: systems that reflect some of the key aspects also present in biology, while sidestepping numerous confounding factors that haunt the analysis of real biomembranes. The availability of such model systems is a major reason for the renewed interest in the question of asymmetry.

Experiments provide the only direct access to nature, but they are also constrained by physical or technical circumstances, such as diffraction limits, control of state- and boundary conditions, or purity of sample preparation. As a partial way around such nuisances, molecular dynamics simulations provide a complementary method of insight into many questions of interest. Provided one accepts the underlying model (not at all a trivial matter, but let us sidestep this discussion here), simulations afford a look at a system's precise state that is unencumbered by many experimental restrictions. Their biggest impediment is the accessible length- and time scales, which may frequently be too small or too short (or both). This has been one of the major driving forces for the development of coarse-grained models[17−22] that strive to capture the essence of a given physical situation simpler and more efficiently, which in turn makes the study of larger systems over longer time scales feasible.

The challenge of balancing accessible system size against required molecular resolution can be nicely illustrated by the case of asymmetric membranes. On the one hand, a model needs to feature enough resolution for the notion of different membrane components to be meaningful; on the other hand, many aspects of asymmetry (say, large scale shape deformations driven by an asymmetric membrane's spontaneous curvature) do not depend on fine chemical detail but only on fairly coarse features: density differences, overall lipid shape, order parameter, *etc*. Hence, asymmetric membranes are a good example where much insight could be gained by relatively low-resolution modeling. However, as one progresses along the axis of ever simpler and more efficient lipid models, an entirely new problem arises that is quite unrelated to the usual question of systematic coarse graining (i.e., how well can we represent the equilibrium phase space distribution of an atomistic system with a smaller number of degrees of freedom[21]). The problem is that coarse grained lipid models tend to have much higher flip-flop rates compared to real systems. What this statement precisely means is actually not entirely trivial in the context of a coarse-grained model, since it requires a discussion of how coarse-grained units map to SI units. We will discuss the essence of this problem in Section 2.5 below.

If we are only interested in equilibrium properties, a strongly increased flip-flop rate need not be a problem; it might at times even be advantageous in order to achieve equilibrium (e.g., when creating vesicles and not having to worry exactly how many more lipids one needs to place in the outer leaflet relative to the inner one, as the correct difference will adjust automatically by flip-flop). However, if we are interested in asymmetric bilayers, and hence wish to study a metastable but fairly long-lived state, it is a distinct problem if its lifetime is significantly cut short—possibly by *many* orders of magnitude, and thus conceivably so short that it cannot be investigated at all.

The problem just described tends to increase in severity as the membrane model decreases in resolution. This is awkward if one is interested in the large-scale implications of asymmetry: the more large-scale the question, the more coarse-grained the model one may wish to use, but the subsequent inability of such models to maintain lipid asymmetry then defeats the original point of the study. Hence, one must either find a way to proceed with a more refined model (i.e., make do with smaller systems or figure out how to run big ones more efficiently) or find a way to suppress flip-flop in highly coarse-grained models. In this paper, we will look at the second strategy. Specifically, we focus on the highly coarse-grained implicit solvent model due to Cooke et al.,[23,24] in which a lipid is represented by three effective beads: one acting as the headgroup and two beads comprising the tail region. This model has been used fruitfully to investigate a wide range of bilayer elastic phenomena and membrane interactions with proteins and nanoparticles in a generic setting, and hence it would be desirable to have a "version" of it that is much better at maintaining an imposed lipid asymmetry, maybe even in cases where a differential stress creates an active driving force for flip-flop.

1.2. How to Suppress Lipid Flip-Flop. Lipid flip-flop is a typical example of an event that requires crossing a free energy barrier.[6] Since for such a process the transition rate depends exponentially on the barrier height,[25,26] the obvious way to strongly increase the lifetime of asymmetric states is to increase this free energy barrier—for instance by including additional interaction potentials that energetically penalize configurations that occur at the transition state but do not contribute significantly to equilibrium states. This is the "kinetic solution" illustrated in the upper right panel of Figure 1. One could, for example, make the interaction between a coarse-grained hydrophilic head-bead and the hydrophobic tail-beads of the bilayer interior even more unfavorable.

This approach to reducing the flip-flop rate, while conceptually straightforward, proves rather difficult in practice for highly coarse-grained models like the Cooke model. With only three beads per lipid to work with, it is very difficult to

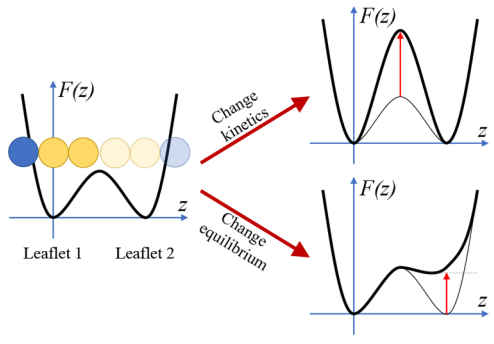

Figure 1. Schematic illustration for the two different ways to stabilize bilayer asymmetry. The curves show a lipid's free energy F as a function of its center of mass coordinate z across the bilayer, with the two minima corresponding to the two leaflets. If the free energy barrier separating them is too low, one can either attempt a *kinetic* fix that artificially increases it or an *equilibrium* fix that artificially increases the free energy of a lipid in the "wrong" leaflet, thus explicitly breaking the symmetry of the situation. For highly coarse-grained systems, the latter approach is more practical.

https://dx.doi.org/10.1021/acs.jctc.0c00862
J. Chem. Theory Comput. 2020, 16, 7195−7206

introduce a force to keep lipids out of the center of the bilayer without detrimentally impacting the equilibrium properties of the original model that made it useful. Stated differently: in such a highly coarse-grained model, transition states are difficult to separate from equilibrium states due to the strongly reduced dimensionality of phase space. Any changes in interaction potentials designed to affect the region in phase space that contains transition states will invariably "spill over" into regions of phase space that describe equilibrium states.

Bearing this in mind, we instead follow a strategy that works by tweaking equilibrium states, as indicated in the lower right panel of Figure 1. The key idea, originally proposed and successfully implemented by Wang, Hu, and Zhang (or "WHZ" in the following), is to label lipids by which leaflet they originally belong to and introduce a penalty for opposite "type" lipids being adjacent in the same leaflet.[27] Observe that this would create a distinction even between chemically identical lipids, since the purpose of the label is to preserve the memory of an initial condition. The goal is to ensure that same-type-lipids residing in the same leaflet interact in a manner identical to the original model, while a lipid flipping into the "wrong" leaflet (meaning, not the one it originally started in) encounters unfavorable interactions with its "wrong" neighbors that drive it back into the "right" leaflet.

The original WHZ-fix for the Cooke model consisted of turning off the attraction between middle beads for lipids belonging to different leaflets. This indeed works; but we will show that once we introduce even a modest differential stress between the two leaflets—a situation that might easily arise in asymmetric membranes[28]—the equilibrium stress asymmetry falls behind the imposed one, and beyond a critical point one even finds domains of the "wrong" lipids residing in their nonhost leaflet, dramatically reducing the imposed asymmetry. We discuss ways for how to quantify and predict this breakdown and propose as a simple solution the introduction of a second "middle" bead, which pushes the breakdown to much higher stress asymmetries. We then measure several key material properties of the modified 4-bead flip-fixed Cooke model and employ it to investigate some examples of asymmetry dependent elastic physics.

2. METHODS

2.1. The Standard Cooke Model. The Cooke model is a highly versatile implicit solvent generic lipid model for simulating bilayer membranes.[23,24,29] Careful measurements of its mechanical properties exist, including the bending rigidity,[24,30,31] Gaussian curvature modulus,[32] pivotal plane position,[33] tilt modulus,[34] and curvature softening;[35] and it has been used to shed light onto a variety of biophysical and biomedical situations, such as curvature[36] and composition[37] mediated interactions, antimicrobial peptide insertion,[38] lipid curvature sorting,[39] dynamin-driven membrane fission,[40] nanoparticle coating,[41] receptor-mediated endocytosis,[42] and soft nanoparticle wrapping.[43]

For ease of reference, let us briefly recount the basics of the model, focusing on the aspects that will be important in understanding the modifications to be made later. A more detailed description of the Cooke model and the rationale behind its design can be found in the original references.[23,24]

Individual lipids are generically represented by a string of three coarse-grained beads: one representing the hydrophilic headgroup and two comprising the tail region. The beads are held together by finite extensible nonlinear elastic (FENE) bonds with interaction potential given by

$$V_{\mathrm{bond}}(r) = -\frac{1}{2}k_{\mathrm{bond}}r_\infty^2 \log\left[1 - \left(\frac{r}{r_\infty}\right)^2\right] \tag{1}$$

where the maximum bond range $r_\infty = 1.5\sigma$, with σ being the unit of length in our coarse-grained system, and $k_{\mathrm{bond}} = 30\varepsilon/\sigma^2$, with ε being the unit of energy. To keep lipids relatively straight, a harmonic spring with rest length 4σ and spring constant $k_{\mathrm{bend}} = 10\varepsilon/\sigma^2$ is used between the head bead and terminal tail bead

$$V_{\mathrm{bend}}(r) = \frac{1}{2}k_{\mathrm{bend}}(r - 4\sigma)^2 \tag{2}$$

The head beads interact through a purely repulsive Weeks-Chandler-Anderson (WCA) potential, given by

$$V_{\mathrm{rep}}(r) = \begin{cases} 4\varepsilon\left[\left(\frac{b}{r}\right)^{12} - \left(\frac{b}{r}\right)^{6} + \frac{1}{4}\right], & r \le r_c \\ 0, & r > r_c \end{cases} \tag{3}$$

with $r_c = 2^{1/6}b$. The original model uses $b_{\mathrm{head,head}} = b_{\mathrm{head,tail}} = 0.95\sigma$, and $b_{\mathrm{tail,tail}} = \sigma$ (see Figure 2).

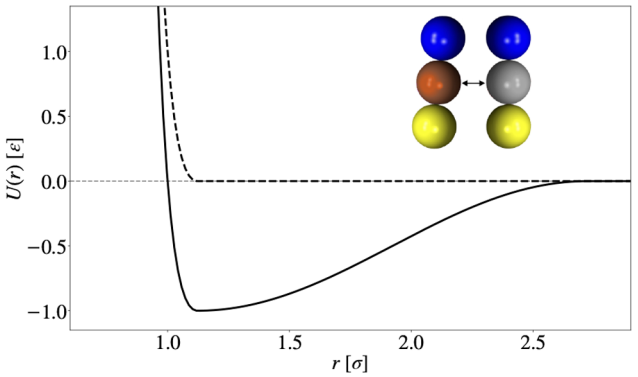

Figure 2. Head-bead interaction potential $V_{\mathrm{rep}}(r)$ (dashed) and tail-tail interaction $V_{\mathrm{rep}}(r) + V_{\cos}(r)$ (solid), plotted for $b = 1.0\sigma$, $w_c = 1.6\sigma$. Inset image: in the WHZ-modified Cooke model, the potential between middle beads that initially belong to opposite leaflets is changed from $V_{\mathrm{rep}} + V_{\cos}$ to V_{rep}.

In the absence of explicit solvent molecules, the hydrophobic effect is mimicked by an extended-range cohesive interaction between the tail beads of the lipid molecules. Especially the tunability of the range is crucial, since a mere Lennard-Jones attraction proved to be too short-ranged to stabilize a fluid phase.[24] As an alternative functional form, Cooke et al.[23] chose a half-period of a cosine, which also allows the potential to go smoothly to zero at a finite range:

$$V_{\cos}(r) = \begin{cases} -\varepsilon, & r < r_c \\ -\varepsilon\cos^2\left[\frac{\pi}{2w_c}(r - r_c)\right], & r_c \le r \le r_c + w_c \\ 0, & r > r_c + w_c \end{cases} \tag{4}$$

The sum $V_{\mathrm{rep}}(r) + V_{\cos}(r)$ yields a smooth (once differentiable) attractive potential similar to the standard LJ interaction but with a range that can be tuned via w_c.

https://dx.doi.org/10.1021/acs.jctc.0c00862
J. Chem. Theory Comput. 2020, 16, 7195−7206

2.2. WHZ Modification. As explained above, the WHZ modification to the Cooke model consists of artificially introducing two different classes of lipids in the two leaflets and eliminating the V_{cos} interaction between the middle beads of opposite-leaflet classes.[27] WHZ needed this modification, because they wanted to measure the spontaneous curvature of a bilayer consisting of different lipids in the two leaflets. To create different regions along the membrane with different spontaneous bilayer curvatures, this also required them to add additional interactions that drove phase separation, which also helped to keep not just the phases but also the "sidedness" intact.

Let us begin by testing the effectiveness of the WHZ modification but under circumstances that add an additional energetic incentive for lipids to flip (beyond the usual entropic one). Specifically, we create a membrane consisting of a single lipid type, divided into two leaflet classes, but we impose slightly different lipid area densities by choosing different numbers N_+ and N_- of lipids for the two leaflet. For the sake of being specific, let us assume $N_+ > N_-$, which means that the ⊕-leaflet is "overfilled" and the ⊖-leaflet is "underfilled". If the whole membrane is under zero net mechanical tension, this implies that the ⊕-leaflet is under compression, while the ⊖-leaflet is under tension; and this creates an incentive for lipids in the ⊕-leaflet to relax this tension by flipping into the ⊖-leaflet.

We performed a set of simulations of WHZ flip-fixed Cooke lipid membranes (at the common state point $k_BT = 1.1\varepsilon$ and $w_c = 1.6\sigma$), always choosing $N_+ + N_- = 800$, but with increasing values for the number difference. We find it convenient to characterize the latter with the asymmetry parameter

$$\delta n := \frac{N_+ - N_-}{N_+ + N_-} \tag{5}$$

Figure 3 shows the outcome: the red triangles mark the average observed asymmetry $\langle \delta n \rangle$ as a function of the imposed one, δn_0. Initially they are identical, but already at $\delta n_0 = 3\%$ the distribution of observed asymmetries has an average that deviates more than one standard deviation from the imposed one. Beyond 5% imposed asymmetry the average observed asymmetry *decreases* with increasing imposed asymmetry, showing that it is impossible to realize an actual asymmetry of more than about 3%—no matter how much one initially overfills the ⊕-leaflet.

This result might look puzzling, and one might even wonder whether the system is in thermal equilibrium. Once asymmetry breaks down, say beyond 5%, could it be that we simply have to wait long enough until enough lipids have flipped out of the overcrowded leaflet and the asymmetry has decayed to zero? The answer is no; the observed asymmetries are indeed equilibrium measurements. To understand this, it is useful to explore in a simple theoretical model what we would expect in such a situation.

If the bilayer were symmetric, each of its two leaflets would host $N_0 = \frac{1}{2}(N_+ + N_-)$ lipids and have an area $A_0 = a_l N_0$, where a_l is the equilibrium area per lipid. (We will ignore higher order corrections due to shape undulations.) Due to the asymmetry δn, the two leaflets individually prefer the unequal areas $A_{0,\pm} = A_0(1 \pm \delta n)$, but they have to compromise to the same area A, which costs the elastic energy

$$E_{stretch}(A) = \frac{1}{2} K_{A,m} \left[\frac{(A - A_{0,+})^2}{A_{0,+}} + \frac{(A - A_{0,-})^2}{A_{0,-}} \right] \tag{6}$$

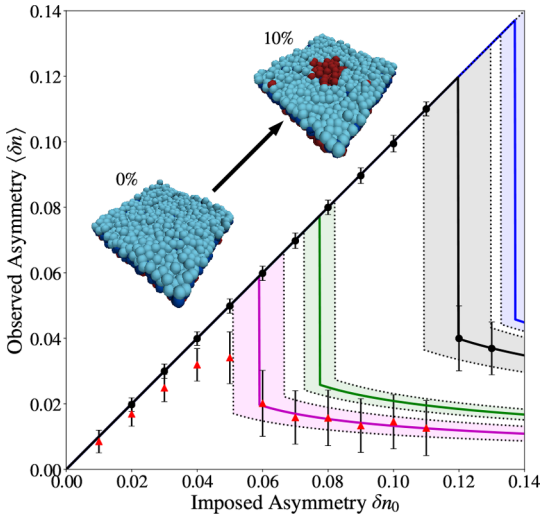

Figure 3. Observed lipid asymmetry $\langle \delta n \rangle$ as a function of imposed one, δn_0. Red triangles: simulation using the WHZ-modified Cooke model (at $k_BT = 1.1\varepsilon$ and $w_c = 1.6\sigma$); the range on each data point indicates the standard deviation of the observed asymmetry, not the error of its mean. Magenta curve: fit of eq 11 in the regime of breakdown to the WHZ data; the shaded region indicates one standard deviation in the fitting parameter. Green curve: again eq 11 but plotted instead of using measured values of γ and $K_{A,m}$ from separate simulations. Black circles: average asymmetry measured in simulation using our new 4-bead flip-fixed Cooke model (at $k_BT = 1.4\varepsilon$ and $w_c = 1.6\sigma$). Black curve and blue curve: same as magenta and green, respectively, but for the 4-bead flip-fixed system. All simulations were done with systems containing 800 lipids. Inset images: two simulation snapshots of 3-bead WHZ-fixed membranes at $\delta n_0 = 0\%$ (left) and $\delta n_0 = 10\%$ (right), illustrating the formation of a domain of ⊕-leaflet lipids (dark red) in the ⊖-leaflet (light blue) upon crossing the critical asymmetry. Head beads are not rendered to allow a clear view of the domain. The snapshots were visualized with VMD.[44]

where $K_{A,m}$ is the area expansion modulus of a single leaflet. If the net tension $\Sigma = \partial E_{stretch}/\partial A$ vanishes, the membrane settles at an area equal to the harmonic mean of $A_{0,+}$ and $A_{0,-}$ and has elastic energy $K_{A,m} A_0 \delta n^2$.

A breakdown of imposed asymmetry means that some number ΔN of lipids move from the overcrowded upper leaflet into the underfilled lower one. This will relax the elastic energy, but in our model, ⊕-side lipids incur an energetic penalty for being a neighbor to ⊖-side lipids. Ignoring entropy of mixing (which is justified at sufficiently high contact penalty), the ΔN lipids then form a single domain of circumference $C = \sqrt{4\pi a_l \Delta N}$ (assuming it is circular), which has an associated line energy

$$E_{line} = \gamma C = \gamma \sqrt{4\pi A_0 (\delta n_0 - \delta n)} \tag{7}$$

where γ is the line tension that a domain of ⊕-lipids residing in the ⊖-leaflet experiences with its ⊖-neighbors, and δn_0 is the initially imposed asymmetry before breakdown. It is important to bear in mind that this line tension γ is an artificial one: it only arises once asymmetry has broken down and a "wrong" domain has formed in the opposing leaflet. It is not to be confused with *physical* line tensions arising in simulation due to contact between chemically distinct lipid species. As it stands thus far, the two "different" lipid types are merely artificial labels used to maintain asymmetry; they represent chemically identical lipids in the two leaflets.

https://dx.doi.org/10.1021/acs.jctc.0c00862
J. Chem. Theory Comput. 2020, 16, 7195−7206

The total energy $E = E_{\text{stretch}} + E_{\text{line}}$ is

$$\frac{E(\delta n, \delta n_0)}{K_{A,\text{m}} A_0} = \delta n^2 + \sqrt{\frac{4\pi\lambda^2}{A_0}(\delta n_0 - \delta n)} \tag{8}$$

where we introduced the important characteristic length

$$\lambda := \frac{\gamma}{K_{A,\text{m}}} \tag{9}$$

To find the equilibrium domain size ΔN—or equivalently, the optimal asymmetry δn that remains after transitioning ΔN lipids—we must minimize E with respect to δn. It is easy to see that $\delta n = 0$ is always at least locally stable, even though $\partial E/\partial\, \delta n$ does not vanish there (it is a boundary minimum). Requiring the derivative to vanish then leads to a cubic equation, the solution of which can be written succinctly using trigonometric functions. Defining the two characteristic asymmetries

$$\delta n_{\text{c}} := \frac{3}{2}\left(\frac{\pi\lambda^2}{2A_0}\right)^{1/3} \tag{10a}$$

$$\delta n_{\text{b}} := 2^{1/3}\delta n_{\text{c}} \tag{10b}$$

one finds that two new extrema arise beyond the *critical* asymmetry δn_{c}

$$\frac{\delta n_{\pm}}{\delta n_0} = 1 - \frac{4}{3}\cos^2\frac{\pi \pm \arccos[(\delta n_{\text{c}}/\delta n_0)^{3/2}]}{3} \tag{11}$$

of which δn_+ is a local maximum and δn_- is a local minimum. The latter becomes a global minimum beyond the *breakdown* asymmetry δn_{b}, at which point the observed asymmetry discontinuously drops by exactly a factor of 3. The domain size at breakdown is then

$$\begin{aligned}\Delta N_{\text{b}} &= N_0(\delta n_0 - \delta n_-)|_{\text{breakdown}} \\ &= N_0\left(\delta n_{\text{b}} - \frac{1}{3}\delta n_{\text{b}}\right) = N_0\left(\frac{\pi\lambda^2}{A_0}\right)^{1/3}\end{aligned} \tag{12}$$

Curiously, both the critical and the breakdown asymmetry depend on the overall membrane area A_0, in such a way that it is more difficult to maintain asymmetry for larger membranes, even though the dependence is relatively weak. Observe that γ and $K_{A,\text{m}}$ only enter in the combined ratio $\lambda = \gamma/K_{A,\text{m}}$, which is the single control parameter of this theory.

The magenta curve in Figure 3 shows a fit of $\delta n_-(\delta n_0)$ from eq 11 to the red triangle in the breakdown regime, using λ as the single fitting parameter. The equilibrium membrane area for the symmetric system of 800 lipids is $A_0 \approx 466\sigma^2$. We find $\lambda = (0.1 \pm 0.01)\sigma$ and $\delta n_{\text{b}} \approx 6\%$. The decline of observed asymmetry with increasing imposed asymmetry (for large asymmetry proportional to $1/\sqrt{\delta n_0}$) is captured very well. However, the observed transition is smeared out compared to the sharp transition, likely because the critical domain is fairly small ($\Delta N_{\text{b}} \approx 17$ in simulation, which agrees with eq 12), and we hence must expect corrections to the line energy and fairly sizable fluctuations.

Instead of fitting λ, we can independently measure line tension γ and area modulus $K_{A,\text{m}}$ in fairly straightforward simulations. For the WHZ-modified 3-bead Cooke model, we find $\gamma = (2.3 \pm 0.1)\varepsilon/\sigma$ and $K_{A,\text{m}} = (16 \pm 1)\varepsilon/\sigma^2$, which leads to $\lambda = (0.14 \pm 0.01)\sigma$. From this we can predict the breakdown behavior, shown as the green curve in Figure 3. The resulting critical asymmetry is about 30% bigger than the one inferred from the fit, which could again indicate difficulties with the small domain size, but overall this gives a remarkably close prediction for when we must expect an imposed asymmetry to catastrophically fail. This knowledge is useful in order to determine ahead of time whether a desired asymmetry δn will be sustainable in a membrane of size A_0. Eq 10a implies the following upper bound for membrane size:

$$A_0 < \frac{\pi\lambda^2}{(2\delta n_0/3)^3} \tag{13}$$

As a side note, the lipid domain breakthrough we have investigated here is closely related to the physics of pore-opening in a stressed membrane under *constant strain*. Indeed, the theory we have presented here is essentially identical to the one that has previously been developed for the pore-opening scenario.[24,45,46]

2.3. Improving the Flip Suppression. The data in Figure 3 show that the WHZ modification of the standard Cooke model, while in principle working, is not strong enough to maintain even a moderate differential stress—one important way in which a bilayer could be asymmetric, and hence a reason why one might wish to suppress lipid flip-flop in the first place. However, our theoretical model from the previous section indicates how to remedy this shortfall: since both the critical and the breakdown asymmetry are proportional to $\lambda^{2/3} = (\gamma/K_{A,\text{m}})^{2/3}$, we can try to either increase the line tension γ or decrease the area expansion modulus $K_{A,\text{m}}$. Of those two, the expansion modulus is a physical material parameter we might wish to independently tune, while the line tension is only related to the artificial distinction between the two leaflet classes. Attempts to increase γ will not (to lowest order) affect other desirable membrane properties, and so this is the path we follow.

2.3.1. Additional Repulsive Interactions Do Not Help. The line tension γ increases if we make the interaction between top and bottom leaflet class lipids even more unfavorable. Considering that the midbead attraction has already been completely turned off, and we cannot turn off the interaction between tail-end beads (because then the two leaflets unbind), one might try to further amplify the incompatibility by adding an explicit repulsion. This, however, does not work, and it is instructive to see why not.

The key point is that attractions and repulsions affect lipid configurations very differently. Increasing the attraction between two neighboring Lennard-Jones particles lowers the energy as much as one likes, but increasing their repulsion need not increase the energy. Instead, it may merely push the particles further apart, and under conditions of zero applied pressure this costs no energy (to lowest order). In the membrane case, the situation is slightly more complicated, because even if the entire bilayer is under zero tension, a flip-event of a lipid into the wrong leaflet still creates a differential strain between the two leaflets that costs energy. However, the fact that a local repulsion becomes "collectivized" as a global strain implies that the net energy change shows a strong finite size dependence. Using the elastic model of two coupled leaflets as given in eq 6, with $A_{0,+} = (N_0 - 1)a_l$ and $A_{0,-} = N_0 a_l + a_l'$, where $a_l' > a_l$ is the area a $\oplus$-lipid requires when it flips into the $\ominus$-leaflet, we find that the overall energy change of such a flip is proportional to $1/A_0$; and while the WHZ fix itself also has a finite size effect, as seen in eq 10a and eq 12, the resulting exponent is much weaker ($-1/3$ as opposed to -1). Even worse, this repulsion-induced energy change of a $\oplus$-lipid flipping into the $\ominus$-leaflet is entirely undone

https://dx.doi.org/10.1021/acs.jctc.0c00862
J. Chem. Theory Comput. 2020, 16, 7195−7206

if additionally a ⊖-lipid flips into the ⊕-leaflet. Instead of penalizing two incorrectly placed lipids, this pair exchange cancels the cost due to repulsive interactions. Working with repulsions is not the way to go.

2.3.2. Adding One More Bead to the Cooke Model. We instead provide ourselves some extra material to work with by augmenting our coarse-grained lipids with an additional tail bead. With four beads per lipid, we now have two middle beads whose cross-type interactions can be modified, allowing us to more than double the energy penalty for neighboring opposite-type lipids by removing their cohesive interaction energy as in the WHZ modification. Figure 4 diagrams the interactions defined between the different bead types of our 4-bead lipids.

	1	2	2	3	6	5	5	4
1	0.95 no	0.95 no	0.95 no	0.95 no	0.95 no	0.95 no	0.95 no	0.95 no
2	0.95 no	1.0 yes	1.0 yes	1.0 yes	1.0 yes	1.0 **no**	1.0 **no**	0.95 no
2	0.95 no	1.0 yes	1.0 yes	1.0 yes	1.0 yes	1.0 **no**	1.0 **no**	0.95 no
3	0.95 no	1.0 yes	1.0 yes	1.0 yes	1.0 yes	1.0 yes	1.0 yes	0.95 no
6	0.95 no	1.0 yes	1.0 yes	1.0 yes	1.0 yes	1.0 yes	1.0 yes	0.95 no
5	0.95 no	1.0 **no**	1.0 **no**	1.0 yes	1.0 yes	1.0 yes	1.0 yes	0.95 no
5	0.95 no	1.0 **no**	1.0 **no**	1.0 yes	1.0 yes	1.0 yes	10 yes	0.95 no
4	0.95 no	0.95 no	0.95 no	0.95 no	0.95 no	0.95 no	0.95 no	0.95 no

Figure 4. Interaction matrix between all beads of the two classes of a 4-bead flip-fixed Cooke model. Beads 1, 2, and 3 belong to the ⊕-lipid class (i.e., upper leaflet), and beads 4, 5, and 6 belong to the ⊖-lipid class (i.e., lower leaflet). Bead types 1 and 4 are lipid heads. In the table, the upper row indicates the bead-bead interaction size parameter b (from eq 3) in units of σ, and the lower row indicates whether an attractive interaction is turned on. Turning off the attractions between bead types 2 and 5 constitutes the WHZ flip-fix.

The original Cooke model used a harmonic potential between head and tail beads in place of a bond angle potential in order to maintain an approximately linear configuration of the beads. When extending the model to include a fourth lipid bead, this potential is still present between the first (head) bead and the third bead, as well as duplicated between the second bead and the fourth (final tail) bead.

Adding an additional bead to each lipid increases the attractive cohesion between neighboring lipids of the same type. As such, if one simulates this 4-bead model at the same temperature $k_BT = 1.1\varepsilon$ that has become standard for fluid Cooke membrane simulations with $w_c = 1.6\sigma$, one discovers that the membrane is thoroughly in the gel phase. Addition of a fourth bead hence requires a move to a new state point representative of the fluid phase. We find that $k_BT = 1.4\varepsilon$ (at $w_c = 1.6\sigma$) is at a high enough temperature to bring us above the gel transition, while simultaneously permitting large values of the asymmetry parameter δn.

The black circles in Figure 3 show the measured values of asymmetry for this state point plotted against the imposed asymmetry. The membrane maintains nearly perfect asymmetry at the imposed value of δn_0 all the way up to 11%, while beyond that point the flip-suppression breaks down, as seen for the $\delta n_0 =$ 12% and 13% state points. Asymmetries this high are already well beyond what is believed to be of biological relevance. However, it is reassuring that the model can be pushed beyond what is necessary, knowing that a simulation is not on the verge of model failure and asymmetry breakdown. To this end, we also measured the line tension $\gamma = (6.7 \pm 0.2)\varepsilon/\sigma$ and area modulus $K_{A,m} = (19.9 \pm 0.7)\varepsilon/\sigma^2$ in order to use eq 10a to predict an approximate breakdown threshold for our new setup. Based on these measurements, we find $\delta n_c \approx 11\%$ and $\delta n_b \approx 14\%$ for the 800 lipids system shown in Figure 3. More generally, we can use eq 13 to predict that the area for which an imposed symmetry δn_0 remains stable is limited to $A/\sigma^2 \lesssim \delta n_0^{-3}$. Notice, though, that the breakdown threshold predicted in this way appears to be slightly larger than the true value observed for both systems investigated here, as made clear in Figure 3.

2.4. MD Simulations. Molecular dynamics simulations were performed using the ESPResSo package.[47] Constant temperature simulations were carried out using a Langevin thermostat with a friction constant of $\Gamma = 1.0\,\tau^{-1}$ and a time step $\delta t = 0.005\tau$. Constant tension simulations were performed using a modified Andersen barostat[48] allowing isotropic box size changes only in the x- and y-directions. For constant-tension simulations in the vicinity of the gel transition temperature, a rectangular box with length equal to twice its width was used, with box size changes allowed only along the long direction of the box.

2.5. Mapping of Coarse-Grained Scales to Real Units. When simulating a coarse-grained representation of a physical system, the exact meaning of length- and especially time-scales requires a mapping onto the physical unit scale by way of comparing suitable observables of the coarse-grained representation to the real system. This is usually not a problem for "length" or "mass", since the size or mass of a coarse-grained unit can be directly matched to the real-world structure it is supposed to represent. Not so for "time". Formally, we have a coarse-grained time unit τ in a simulation that can be translated into SI units via the equation $\tau = L\sqrt{M/E}$, where $\{L, M, E\}$ are the length-, mass-, and energy-units in a simulation (all of which are straightforward to map); and while this unit is appropriate for "instantaneous" observables that still require the notion of time (such as the kinetic energy), it does not correctly describe the long-time dynamics of the coarse-grained system.

The deeper issue with dynamical observables is that statistical partition functions, and hence free energies, are agnostic about time, and even if the coarse-grained system has been constructed so as to reproduce thermal equilibrium, this does not guarantee that it inherits any meaningful notion of time in the process. Indeed, it *cannot*, because specifying an energy functional does not also specify the equations of motion one wishes to solve. Hence, time-mapping tends to be done explicitly afterward, by observing a particular dynamical process of interest, quantifying it via the "naïve" time unit τ, and then matching this to the SI scale by comparing it to the actual situation.

Let us make a concrete example. The standard Cooke model (at $k_BT = 1.1\varepsilon$ and $w_c = 1.6\sigma$; see Section 2.1 for the definition of those parameters) has an area per lipid of $a_l = 1.2\sigma^2$.[24] Equating this to a typical experimental value of $a_l = 0.65$ nm^2 gives the length mapping $\sigma = 0.74$ nm. The model also has a diffusion constant of $D \approx 0.02\sigma^2/\tau$ (under Langevin dynamics with a friction constant of $\Gamma = \tau^{-1}$).[24] If we naïvely take τ from the bare mapping $\tau = \sigma\sqrt{M/\varepsilon}$ (using $3M = 800$ Da, the mass of a typical

https://dx.doi.org/10.1021/acs.jctc.0c00862
J. Chem. Theory Comput. 2020, 16, 7195−7206

lipid), we find $\tau \approx 8$ ps and hence $D \approx 1400\ \mu m^2/s$—which is *much* larger than what is found experimentally for ordinary fluid-phase lipids: $D \sim 5\ \mu m^2/s$.[49] This is what is meant by "CG dynamics is sped up". A better approach is to map τ by insisting that a CG dynamic variable, such as the diffusion constant, agrees with its experimental counterpart. In the present case, this yields the much longer time unit $\tau \simeq 2$ ns. The problem with this strategy is that the dynamical process to be used for mapping is not unique. For instance, the Cooke model also exhibits lipid flip-flop, with a rate determined to be $r_f \approx 1.32 \times 10^{-4}\ \tau^{-1}$.[24] Together with the diffusion-based time mapping, this implies a rate in SI units of $r_f \simeq 6.6 \times 10^4\ s^{-1}$ or a characteristic time for flip-flop of 15 μs. Since the *actual* time is at least several hours, the flip-flop rate is too large by at least 9 orders of magnitude. This is what is meant by "different dynamical processes are sped up differently".

As a side note, there *is* a way to claim flip-flop is sped up without having to actually map time to SI units, and that is to divide out the two time scales of flip-flop and diffusion. One way to do this is to answer the question, "how far does a lipid on average diffuse before it flips?". The answer is $\Delta x_f = \sqrt{4D/r_f}$, an expression in which the time units in D and r_f cancel. Using the experimental values $D = 5\ \mu m^2/s$ and taking $r_f^{-1} = 1$d, we get $\Delta x_f = 1.3$ mm. With the simulation parameters $D = 0.02\sigma^2/\tau$ and $r_f^{-1} = 10^4\tau$, we instead find $\Delta x_f \approx 28\sigma \approx 21$ nm. We hence see that in experimental systems the flip-diffusion length is about 60000 times larger than for the 3-bead Cooke model.

3. RESULTS

3.1. Measured Observables. As this model is to be used to carry out simulations similar to those performed by the original Cooke model, with the added ability to support differentially stressed membranes, we collect in Table 1 a brief comparison of common observables of interest for the original Cooke model and the 4-bead flip-fixed modification at the chosen state for fluid simulation. Brief explanations of the methods used to calculate these values are given in the Supporting Information. This table does not contain every single observable ever measured for the Cooke model, and so we wish to emphasize that if an observable is not listed, this is *not* meant to imply that its value is identical between the two models. Keep in mind that the observables in Table 1 all come from simulations of *symmetric* membranes, such that a meaningful comparison between the two models can be made. Upon the introduction of asymmetry in the new model, some of these values will change and indeed be different between the two leaflets of the bilayer.

Table 1. Comparison of Observables in the Original 3-Bead Cooke Model and the 4-Bead Flip-Fixed Cooke Model[d]

observable	units	original Cooke	modified Cooke
k_BT_{gel}	ε	0.95 ± 0.03[24]	1.32 ± 0.01
d	σ	4.372 ± 0.002	6.328 ± 0.001
a_l	σ^2	1.206 ± 0.001	1.163 ± 0.001
$K_{A,m}$	k_BT/σ^2	12.1 ± 0.4	14.2 ± 0.1
κ^a	k_BT	12.5 ± 1[30]	30.9 ± 0.2
κ^b	k_BT	13.8 ± 0.4[50]	31.5 ± 1.9
l	σ	4.7 ± 0.8[50]	10.7 ± 1.8
$\kappa_{t,eff}$	k_BT/σ^2	n.d.	11.9 ± 0.4
P_2	1	0.73 ± 0.01	0.82 ± 0.01
γ	ε/σ	2.3 ± 0.1[c]	6.7 ± 0.2
η_K	1	n.d.	1.96 ± 0.03
D	$10^{-2}\sigma^2/\tau$	1.85 ± 0.05	1.69 ± 0.05
r_f	$10^{-4}/\tau$	1.32 ± 0.02	N/A

[a]Determined from fluctuation spectra. [b]Determined from buckling. [c]This includes the WHZ modification. [d]Material properties for original Cooke are given at $k_BT = 1.1\varepsilon$, and properties for the 4-bead model are given at $k_BT = 1.4\varepsilon$; both use $w_c = 1.6\sigma$. The observables are as follows: T_{gel}: gel transition temperature; d: head-to-head bilayer thickness; a_l: area per lipid; $K_{A,m}$: area expansion modulus for a single leaflet; κ: curvature modulus; l: curvature softening length (see eq (SI 1)); $\kappa_{t,eff}$: effective tilt modulus (see eq (SI 4)); P_2: lipid order parameter (see eq (SI 7)); γ: line energy for a domain of lipids belonging to the wrong leaflet (see eq 7); η_K: strain dependence of area modulus (see eq 19b); D: lipid (self) diffusion constant; r_f: flip-flop rate.

Given that the most obvious structural change of our new model is its increased thickness, it is instructive to see how much of the changed elastic behavior can be attributed to this. Simple continuum thin-plate theory states that the area modulus $K_{A,m}$ can be expressed in terms of the Young's modulus E, the monolayer thickness $d/2$, and the Poisson ratio ν as $K_{A,m} = Ed/4(1-\nu)$.[51] Assuming that E and ν are approximately the same in the two models, the ratio between the two area moduli is simply determined by the ratio of the two leaflet thicknesses. More precisely, we find a factor of $(d_4/d_3) \times (k_BT_3/k_BT_4) = (6.328/4.372) \times (1.1/1.4) \approx 1.14$, yielding a prediction of $K_{A,m} \approx 13.8\ k_BT/\sigma^2$ for the area modulus of our new model. The factor of 1.1/1.4 enters from the conversion of k_BT units due to the models being simulated at different temperatures. This is fairly close to the true measured value shown in the table. A similar line of reasoning, this time exploiting the continuum relation $\kappa = Ed^3/(48(1-\nu^2))$, shows that (at fixed E and ν) the bilayer bending modulus is proportional to the cube of the bilayer thickness, leading to the prediction that our new model's bending modulus should be approximately 2.4 times larger than that of the original Cooke model. Taking a rough value of $13k_BT$ for the original Cooke modulus, this gives $\kappa \approx 31k_BT$ for the new one—remarkably close to the actual measurement. While these simple arguments ignore many details, they do suggest that the changes in $K_{A,m}$ and κ are mostly associated with the change in thickness that resulted from adding one more bead.

Let us take the time and briefly map some of the 4-bead coarse-grained observables in that table into SI units. We begin with length, which we map to the area per lipid. Its value depends on lipid type, but a reasonable average value is 0.65 nm^2. Setting $1.16\sigma^2 = a_l = 0.65$ nm^2, we get $\sigma \simeq 0.75$ nm. This would imply a bilayer thickness of $d = 6.328 \cdot (0.75\ \text{nm}/\sigma) = 4.75$ nm. Since this thickness is measured from head bead to head bead, it is appropriate to compare it to experimental phosphate-phosphate bilayer thicknesses. Our membrane then appears to be thicker than most common lipid bilayers, although it is thinner than DNPC bilayers.[52] Using the thermal energy as the point of reference for energy mapping, we get $\varepsilon \simeq k_BT/1.4$. If we, for instance, pick the temperature in k_BT to correspond to body temperature, $T_b = 310$ K, this implies that the gel transition happens at $T_{gel} = (1.32/1.4)T_b = 0.943T_b = 292$ K = 20 °C.

Having mapped length and energy, we can now translate the monolayer expansion modulus: $K_{A,m} = 19.9\varepsilon/\sigma^2 = 14.2\ k_BT_b/\sigma^2 = 108$ mN/m. This gives $K_A = 216$ mN/m for the bilayer expansion modulus, which is only about 10% smaller than the value found for a wide range of phospholipids.[53] For the effective tilt modulus, we get $\kappa_{t,eff} = 11.6k_BT_r/\sigma^2 = 88$ mN/m, but we cannot easily compare this to the actually measured tilt modulus due to corrections related to its "effective" nature (see refs 54 and 55 for details); but to see that the order of magnitude is

https://dx.doi.org/10.1021/acs.jctc.0c00862
J. Chem. Theory Comput. 2020, 16, 7195−7206

meaningful, we note the tilt modulus of DOPC (dioleoylphosphatidylcholine) at 30 °C was recently determined to be $\kappa_t = 95 \pm 7$ mN/m,[56] and probing a wider set of lipids indicates that the modulus varies between about 40 mN/m and 100 mN/m.[57]

Finally, we can map time via lipid self-diffusion, using a common value for the diffusion constant of 5 $\mu m^2/s$.[49] From $1.69 \times 10^{-2}\sigma^2/\tau = D = 5\ \mu m^2/s$ and our previous length scale mapping, we get $\tau \simeq 1.9$ ns. Given the difficulties of time-mapping and the range of real diffusion constants, this should best be taken as merely an order-of-magnitude estimate.

3.2. Applications. Having described our method for suppressing flip-flop and demonstrating its effectiveness, we now provide two example applications which illustrate simulations that were inaccessible to the original Cooke model.

3.2.1. Determining $K_{A,m}$ from the Lateral Stress Profile. An important physical object from which many useful observables can be calculated is a membrane's lateral stress profile.[58] Consider a flat, laterally homogeneous membrane spanning the xy-plane with its normal along the z-direction. The stress tensor σ_{ij} is evidently diagonal in these coordinates and due to translational symmetry can only depend on z. The lateral stress profile is then defined as

$$\sigma(z) = \left\langle \frac{1}{2}[\sigma_{xx}(z) + \sigma_{yy}(z)] - \sigma_{zz}(z) \right\rangle \tag{14}$$

Mechanical stability requires $\langle \sigma_{zz}(z) \rangle$ to be constant and hence equal to the bulk pressure[59] (which is zero in our solvent-free coarse-grained model). This provides a good check for the stress calculation.

We measure $\sigma(z)$ in simulations using the Irving-Kirkwood formalism, as presented in great detail by Hardy,[60,61] with the exception that the kinetic contribution to the stress tensor is replaced by its equilibrium average value. In order to ensure that $z = 0$ corresponds to the bilayer midplane, care must be taken when defining the coordinate system. Simply using the bilayer center of mass as the origin of z would result in $z = 0$ being located within the tail region of the overfilled leaflet, rather than at the interface between the two monolayers. In our analysis, the midplane is determined by averaging the z-positions of the final tail beads of the lipids in each leaflet separately and then taking the midpoint between the two resulting values. The lateral stress is evaluated at 61 evenly spaced points in the z-interval from -5σ to 5σ, and the error on these values is calculated via blocking.[62] Figure 5 shows a sequence of lateral stress profiles, determined from simulations of a flip-fixed 4-bead Cooke model membrane with 256 lipids in total and an increasing asymmetry δn, under conditions of overall vanishing bilayer tension—meaning, a vanishing integral of $\sigma(z)$. As was true for the standard Cooke model, this stress profile again looks "flipped" compared to more realistic lipid models, since bilayer cohesion is driven by tail attraction, while the head groups repel. This yields a positive (i.e., attractive) stress in the tail regions and two negative (i.e., repulsive) peaks near the positions of the heads. The most obvious asymmetry-induced changes to the stress profile occur in that head region: the overfilled leaflet (positive z) experiences increasingly stronger head repulsions, while these correspondingly decrease in the underfilled leaflet (negative z), as illustrated by the arrows in Figure 5. Weaker trends along the same lines are seen in the tails. A closer look also reveals that the compressed leaflet slightly increases in thickness, while the expanded leaflet thins. This is expected based on volume conservation, which holds almost perfectly for real bilayers.[63]

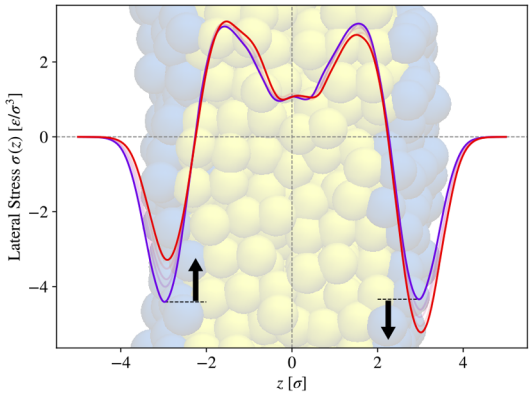

Figure 5. Lateral stress profile as a function of transverse coordinate z in a flat asymmetric Cooke membrane. Each curve corresponds to a different amount of asymmetry, with the symmetric ($\delta n = 0$, purple) and largest asymmetry ($\delta n \approx 8\%$, red) cases being shown darker than the intermediate values. The bilayer midplane is located at $z = 0$. As asymmetry increases, the lipid number decreases in the lower leaflet (negative z values) and increases in the upper leaflet (positive z values).

Moments of this stress profile can be related to a variety of curvature elastic moduli and quantities of interest.[54,55,64−66] Here we will merely examine the zeroth moment (i.e., the integral of the stress profile), but restricted to individual leaflets, in order to measure the monolayer area modulus $K_{A,m}$ in a way that was not possible in the original Cooke model and which does not require stretching the entire membrane.

From eq 6, we see that the elastic energy $E_\pm$ of an individual $\oplus$- or $\ominus$-leaflet is given by

$$E_\pm(A) = \frac{1}{2}K_{A,m}\frac{(A - A_{0,\pm})^2}{A_{0,\pm}} \tag{15}$$

and therefore the lateral mechanical tension is

$$\Sigma_\pm(A) = \frac{\partial E_\pm(A)}{\partial A} = K_{A,m}\frac{A - A_{0,\pm}}{A_{0,\pm}} \tag{16}$$

As mentioned before, the condition of zero overall bilayer tension combined with the coupled bilayer energy in eq 6 tells us that the membrane area A will relax to the harmonic mean of $A_{0,+}$ and $A_{0,-}$. If we substitute this into eq 16 and write the area in terms of δn, we arrive at a very compact expression for the tension in an individual monolayer of an asymmetric membrane under conditions of zero bilayer tension:

$$\Sigma_\pm(\delta n, \Sigma = 0) = \left(\frac{\partial E_\pm}{\partial A}\right)_{\Sigma=0} = \mp K_{A,m}\delta n \tag{17}$$

By integrating the measured stress profile in simulations of membranes under zero tension and varying asymmetry, we can therefore extract the monolayer area modulus through a simple linear fit, as is shown in Figure 6. The error bars for each monolayer tension value are determined by integrating resampled stress profiles for the corresponding asymmetry value. We find a value of $K_{A,m} = (19.8 \pm 0.2)\varepsilon/\sigma^2$.

We note in passing that this procedure directly measures the area modulus of the monolayer, instead of inferring it from the bilayer modulus. This is potentially interesting in light of recent work that has cast doubt on the relation $K_A = 2K_{A,m}$;[67] but since we independently find $\frac{1}{2}K_A = (20.8 \pm 0.7)\varepsilon/\sigma^2$ from a bilayer stretching experiment, our two measurements are entirely

https://dx.doi.org/10.1021/acs.jctc.0c00862
J. Chem. Theory Comput. 2020, 16, 7195−7206

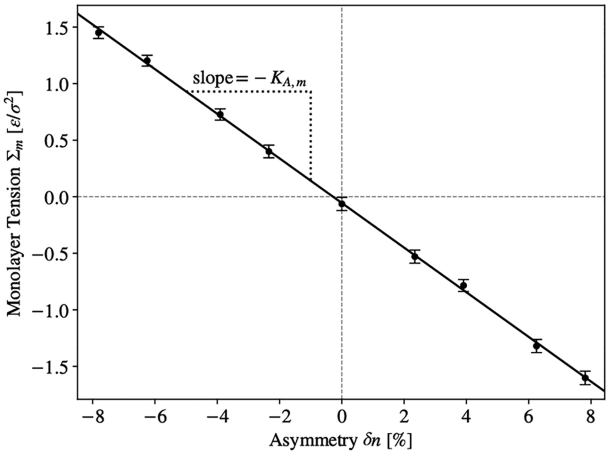

Figure 6. Monolayer surface tension $\Sigma_\pm$ as a function of bilayer asymmetry δn. Each data point is obtained by integrating half of the corresponding stress profile shown in Figure 5. Underfilled and overfilled monolayers are plotted with negative and positive δn values, respectively.

compatible with the common notion that leaflet stretching moduli simply add. (The probability that the observed difference happens by chance is about 17%, determined by integrating the tails of the distribution of the difference between our two measurements, assumed to be Gaussian.)

3.2.2. Bilayer Resting Area as a Sensitive Probe of the Strain-Dependent Area Modulus $K_{A,m}$. Consider again the simple stretching energy for a bilayer, eq 6. Minimizing it with respect to area yields the equilibrium (or "resting") area A_{eq} of the membrane as a function of asymmetry δn, and from this we get the relative area change with respect to the symmetric resting area A_0:

$$\alpha := \frac{A_{eq} - A_0}{A_0} = -\delta n^2 \tag{18}$$

However, Figure 7 shows that this qualitatively disagrees with our observation for the 4-bead flip-fixed Cooke model: instead of shrinking, the area increases with asymmetry.

To understand this disagreement, notice that the predicted effect is actually *quadratic*. To linear order, the asymmetry induced compression in the overfilled leaflet precisely cancels the tension in the underfilled one, leaving the area unchanged. The expansion observed in Figure 7 must therefore result from higher order corrections that are missing in our simple theory. Indeed, our equation assumes that both the compressed and the tense leaflet still have the same stretching modulus $K_{A,m}$, but it seems plausible that the compressed leaflet becomes stiffer, and the tense leaflet become softer. This correction beyond a lowest-order Hookean behavior would shift the area balance in favor of expansion. To account for this, let us permit the area modulus to depend on leaflet strain, $u_\pm \equiv (A_\pm - A_{0,\pm})/A_{0,\pm}$

$$K_{A,m\pm}(u_\pm) = K_{A,m,0} + K_{A,m,1}u_\pm + \cdots \tag{19a}$$

$$= K_{A,m,0}[1 - \eta_K u_\pm + \cdots] \tag{19b}$$

where we have defined the coefficient $\eta_K = -K_{A,m,1}/K_{A,m,0}$, which quantifies the strength of the first nonlinear correction to the leading order Hookean behavior. The sign is chosen such that overcrowding (which corresponds to a *negative* strain) leads to stiffening if η_K is positive.

If we replace $K_{A,m}$ in eq 6 with $K_{A,m\pm}$ from eq 19b, we find the leading order relative area expansion

$$\alpha = \left(\frac{3}{2}\eta_K - 1\right)\delta n^2 + O(\delta n^4) \tag{20}$$

For $\eta_K = 0$, this, of course, reduces to eq 18. Furthermore, as long as $\eta_K < 2/3$, the bilayer area still shrinks when an asymmetry is introduced, even though less strongly. This means that reversing the "naïve" trend requires a minimum amount of nonlinearity. Fitting the expansion observed in Figure 7 to the prediction from eq 20, we find $\eta_K = 1.96 \pm 0.03$ for the flip-fixed 4-bead Cooke model (at $k_BT = 1.4\varepsilon$ and $w_c = 1.6\sigma$).

Observe that the fit works remarkably well, and it permits us to determine a subtle nonlinear correction at a percent-level accuracy, using very simple measurements. One might worry that this really proves the correction to be quite large, which, in turn, might cast doubt on our modeling of the monolayer tension in eq 16, which ignored the nonlinearity.

However, eq 17 shows that the lowest order in the monolayer tension $\Sigma_\pm$ is *linear* in the asymmetry, while for α it is *quadratic*. Whatever nonlinear correction for $\Sigma_\pm$ exists, it needs to compete with a potentially much larger linear term. Indeed, our refined nonlinear theory predicts

$$\Sigma_\pm = \mp K_{A,m}\delta n\left[1 - \frac{3}{2}\eta_K(3\eta_K - 1)\delta n^2 + O(\delta n^4)\right] \tag{21}$$

At the largest asymmetry we studied, $\delta n = 8\%$, the subleading correction term in eq 21 (technically: cubic in δn) is approximately 10% of the leading linear term. Curiously, the quadratic area change term in eq 20 is even smaller, approximately 1%, and hence about ten times smaller than the relative correction to the stress. However, it need not compete with a lower order; it *is* the lowest order. Combining this with the common experience that it is easy to measure lipid areas very precisely, while membrane stress is a much more noisy observable, we conclude that quantifying the asymmetry-induced bilayer area change is a highly sensitive measurement of the small nonlinear correction in a membrane's area expansion behavior.

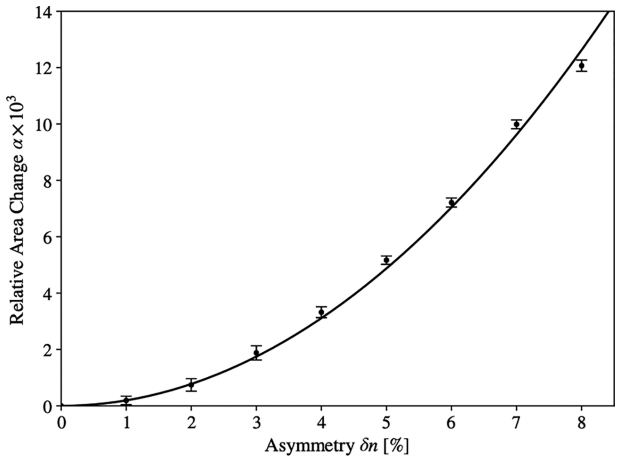

Figure 7. (filled circles) Measurements of relative area change α for the asymmetric Cooke model at $k_BT = 1.4\varepsilon$. (solid line) Fit to eq 20.

4. DISCUSSION AND CONCLUSION

We have presented an extension of the classical Cooke model[23,24] for coarse-grained simulations of lipids, which

https://dx.doi.org/10.1021/acs.jctc.0c00862
J. Chem. Theory Comput. 2020, 16, 7195−7206

combines the ease and efficiency of the original model with the ability to maintain lipid asymmetry, even under conditions of a substantial differential stress. Since the conceptually straightforward attempt to raise the free energy barrier for flip-flop is not viable for highly coarse-grained models, we instead follow the original proposal by Wang et al.:[27] preassign a leaflet-identity to every lipid and then penalize the energy of lipids venturing into the wrong leaflet.

The WHZ fix is successful but only up to a fairly moderate differential stress. We explained why rendering interactions in the wrong leaflet even more unfavorable by adding extra repulsive forces does not work and hence instead added a fourth bead to the lipid, which allows bigger energy differences between lipids in the right and in the wrong leaflet. As a consequence, lipid density asymmetries of up to 10% can be reliably maintained, which is likely large enough for any practical applications.

The additional CG bead, of course, changes the model strongly enough such that all parameters previously determined for the 3-bead Cooke model change upon transitioning to the 4-bead flip-fixed version. For this reason, it made little sense to tune the state point (in terms of k_BT/ε and w_c/σ) such that some parameters (say, area per lipid or bending rigidity) are preserved, since not all parameters could be similarly matched. Instead, we have remeasured the set of most frequently needed physical observables (see Table 1), so that future users have them readily available (or could check their code implementations against our numbers).

The model remains easy to implement and work with, as it relies exclusively on pair forces. This, in particular, simplifies the calculation of stresses, since the standard virial suffices, and more subtle questions for how to parse out multibody interactions (such as bending potentials or dihedrals) can be avoided.

The additional bead slightly increases the computational cost, and there are two ways how to quantify this. In units of coarse-grained time, we observe that it takes about 68% longer to simulate a given number of τ. Alternatively, if we wish to roughly map this to SI units by matching lipid self-diffusion, the slightly smaller diffusion constant of the 4-bead model ($D_{4b} = 1.69 \times 10^{-2}\sigma^2/\tau$ *vs* $D_{3b} = 1.85 \times 10^{-2}\sigma^2/\tau$) gives another factor of 1.095 during time mapping, meaning that one needs to simulate 74% longer to simulate a given number of seconds. If maintaining asymmetry is crucial for the problem at hand, then this moderate increase is worth paying, and it is still much less than the alternative of using more highly resolved lipid models (such as MARTINI[68]) which, by virtue of their higher resolution, automatically have a lower flip-flop rate.

We illustrated the possibilities opened by such a model with two simple applications. First, we showed how to directly determine the monolayer area expansion modulus $K_{A,m}$ (i.e., without just assuming it is half the bilayer expansion modulus K_A), which hence allowed us to independently verify that $K_A = 2K_{A,m}$; and second, we showed that measuring the change of bilayer area with lipid number asymmetry δn affords a highly sensitive means to assessing the strain dependence of the expansion modulus, i.e., the non-Hookean corrections to area strain elasticity.

Many other applications are conceivable. For instance, creating different lipid types by introducing differences in cohesion energy or -range permits the study of phase separation,[37] and in an asymmetric system, this allows one to study the conditions under which nonideal mixing in one leaflet imprints onto the other. This is a highly relevant question for cellular plasma membranes, which are known to have phase separation potential in their outer leaflet, but the consequences of this (say, protein sorting and colocalization) are mostly believed to play out on the inner leaflet. Changing the relative sizes of head versus tail beads permits the introduction of bilayer curvature (the original application of the WHZ modification[27]), and this also opens a window into the subtle interplay between curvature, differential stress, and residual tension, as recently discussed in ref 28. Membranes can also stiffen in the presence of differential stress,[28] a phenomenon that appears to be related to, but not identical with, the gel transition, and the ability to collect more statistics in highly coarse-grained models (together with the opportunity to verify the generality of such a claim in an even simpler model) might teach us more about the way in which elasticity and phase behavior are coupled in asymmetric membranes. We hope that the model we have introduced here will be a useful computational tool for answering these and many other questions that rely on a sufficiently slow flip-flop rate.

■ ASSOCIATED CONTENT

Supporting Information

The Supporting Information is available free of charge at https://pubs.acs.org/doi/10.1021/acs.jctc.0c00862.

Details on several computational procedures for determining lipid membrane observables, in particular: area per lipid; gel transition temperature; bending modulus; area expansion modulus; orientational order parameter; line tension between opposite leaflet lipids; diffusion constant; and bilayer thickness (PDF)

■ AUTHOR INFORMATION

Corresponding Author

Markus Deserno − *Department of Physics, Carnegie Mellon University, Pittsburgh, Pennsylvania 15213, United States;* orcid.org/0000-0001-5692-1595; Email: deserno@andrew.cmu.edu

Author

Samuel Foley − *Department of Physics, Carnegie Mellon University, Pittsburgh, Pennsylvania 15213, United States;* orcid.org/0000-0003-2681-235X

Complete contact information is available at: https://pubs.acs.org/10.1021/acs.jctc.0c00862

Notes

The authors declare no competing financial interest.

■ ACKNOWLEDGMENTS

M.D. gratefully acknowledges support from the National Science Foundation under grant CHE 1764257. S.F. gratefully acknowledges support from the Pittsburgh Chapter of the ARCS Foundation.

■ REFERENCES

(1) Lodish, H.; Berk, A.; Kaiser, C. A.; Krieger, M.; Bretscher, A.; Ploegh, H.; Amon, A.; Martin, K. C. M. *Molecular Cell Biology*, 8th ed.; W.H. Freeman: New York, NY, 2016.

(2) van Meer, G. Dynamic transbilayer lipid asymmetry. *Cold Spring Harbor Perspect. Biol.* **2011**, *3*, a004671.

(3) Kobayashi, T.; Menon, A. K. Transbilayer lipid asymmetry. *Curr. Biol.* **2018**, *28*, R386−R391.

(4) Lorent, J. H.; Levental, K. R.; Ganesan, L.; Rivera-Longsworth, G.; Sezgin, E.; Doktorova, M.; Lyman, E.; Levental, I. Plasma membranes

are asymmetric in lipid unsaturation, packing and protein shape. *Nat. Chem. Biol.* **2020**, *16*, 644−652.
(5) Contreras, F.-X.; Sánchez-Magraner, L.; Alonso, A.; Goñi, F. M. Transbilayer (flip-flop) lipid motion and lipid scrambling in membranes. *FEBS Lett.* **2010**, *584*, 1779−1786.
(6) Sapay, N.; Bennett, W. F. D.; Tieleman, D. P. Thermodynamics of flip-flop and desorption for a systematic series of phosphatidylcholine lipids. *Soft Matter* **2009**, *5*, 3295−3302.
(7) Sperotto, M. M.; Ferrarini, A. *The Biophysics of Cell Membranes*; Springer: 2017; pp 29−60, DOI: 10.1007/978-981-10-6244-5_2.
(8) Pomorski, T.; Menon, A. K. Lipid flippases and their biological functions. *Cell. Mol. Life Sci.* **2006**, *63*, 2908−2921.
(9) Pautot, S.; Frisken, B. J.; Weitz, D. A. Engineering asymmetric vesicles. *Proc. Natl. Acad. Sci. U. S. A.* **2003**, *100*, 10718−10721.
(10) Hamada, T.; Miura, Y.; Komatsu, Y.; Kishimoto, Y.; Vestergaard, M.; Takagi, M. Construction of asymmetric cell-sized lipid vesicles from lipid-coated water-in-oil microdroplets. *J. Phys. Chem. B* **2008**, *112*, 14678−14681.
(11) Hu, P. C.; Li, S.; Malmstadt, N. Microfluidic fabrication of asymmetric giant lipid vesicles. *ACS Appl. Mater. Interfaces* **2011**, *3*, 1434−1440.
(12) Matosevic, S.; Paegel, B. M. Layer-by-layer cell membrane assembly. *Nat. Chem.* **2013**, *5*, 958.
(13) Cheng, H.-T.; Megha; London, E. Preparation and properties of asymmetric vesicles that mimic cell membranes effect upon lipid raft formation and transmembrane helix orientation. *J. Biol. Chem.* **2009**, *284*, 6079−6092.
(14) Cheng, H.-T.; London, E. Preparation and properties of asymmetric large unilamellar vesicles: interleaflet coupling in asymmetric vesicles is dependent on temperature but not curvature. *Biophys. J.* **2011**, *100*, 2671−2678.
(15) Chiantia, S.; Schwille, P.; Klymchenko, A. S.; London, E. Asymmetric GUVs prepared by MβCD-mediated lipid exchange: an FCS study. *Biophys. J.* **2011**, *100*, L1−L3.
(16) Doktorova, M.; Heberle, F. A.; Eicher, B.; Standaert, R. F.; Katsaras, J.; London, E.; Pabst, G.; Marquardt, D. Preparation of asymmetric phospholipid vesicles for use as cell membrane models. *Nat. Protoc.* **2018**, *13*, 2086.
(17) Müller-Plathe, F. Coarse-graining in polymer simulation: from the atomistic to the mesoscopic scale and back. *ChemPhysChem* **2002**, *3*, 754−769.
(18) Tozzini, V. Coarse-grained models for proteins. *Curr. Opin. Struct. Biol.* **2005**, *15*, 144−150.
(19) Izvekov, S.; Voth, G. A. A multiscale coarse-graining method for biomolecular systems. *J. Phys. Chem. B* **2005**, *109*, 2469−2473.
(20) Voth, G. A. *Coarse-graining of condensed phase and biomolecular systems*; CRC Press: 2008; DOI: 10.1201/9781420059564.
(21) Noid, W. G.; Chu, J.-W.; Ayton, G. S.; Krishna, V.; Izvekov, S.; Voth, G. A.; Das, A.; Andersen, H. C. The multiscale coarse-graining method. I. A rigorous bridge between atomistic and coarse-grained models. *J. Chem. Phys.* **2008**, *128*, 244114.
(22) Peter, C.; Kremer, K. Multiscale simulation of soft matter systems−from the atomistic to the coarse-grained level and back. *Soft Matter* **2009**, *5*, 4357−4366.
(23) Cooke, I. R.; Kremer, K.; Deserno, M. Tunable generic model for fluid bilayer membranes. *Phys. Rev. E* **2005**, *72*, 011506.
(24) Cooke, I. R.; Deserno, M. Solvent-free model for self-assembling fluid bilayer membranes: stabilization of the fluid phase based on broad attractive tail potentials. *J. Chem. Phys.* **2005**, *123*, 224710.
(25) Kramers, H. A. Brownian motion in a field of force and the diffusion model of chemical reactions. *Physica* **1940**, *7*, 284−304.
(26) Hänggi, P.; Talkner, P.; Borkovec, M. Reaction-rate theory: fifty years after Kramers. *Rev. Mod. Phys.* **1990**, *62*, 251.
(27) Wang, H.; Hu, D.; Zhang, P. Measuring the spontaneous curvature of bilayer membranes by molecular dynamics simulations. *Communications in Computational Physics* **2013**, *13*, 1093−1106.
(28) Hossein, A.; Deserno, M. Spontaneous curvature, differential stress, and bending modulus of asymmetric lipid membranes. *Biophys. J.* **2020**, *118*, 624−642.
(29) Deserno, M. Mesoscopic membrane physics: concepts, simulations, and selected applications. *Macromol. Rapid Commun.* **2009**, *30*, 752−771.
(30) Harmandaris, V. A.; Deserno, M. A novel method for measuring the bending rigidity of model lipid membranes by simulating tethers. *J. Chem. Phys.* **2006**, *125*, 204905.
(31) Hu, M.; Diggins IV, P.; Deserno, M. Determining the bending modulus of a lipid membrane by simulating buckling. *J. Chem. Phys.* **2013**, *138*, 214110.
(32) Hu, M.; Briguglio, J. J.; Deserno, M. Determining the Gaussian curvature modulus of lipid membranes in simulations. *Biophys. J.* **2012**, *102*, 1403−1410.
(33) Wang, X.; Deserno, M. Determining the pivotal plane of fluid lipid membranes in simulations. *J. Chem. Phys.* **2015**, *143*, 164109.
(34) Wang, X.; Deserno, M. Determining the lipid tilt modulus by simulating membrane buckles. *J. Phys. Chem. B* **2016**, *120*, 6061−6073.
(35) Diggins IV, P.; McDargh, Z. A.; Deserno, M. Curvature softening and negative compressibility of gel-phase lipid membranes. *J. Am. Chem. Soc.* **2015**, *137*, 12752−12755.
(36) Reynwar, B. J.; Illya, G.; Harmandaris, V. A.; Müller, M. M.; Kremer, K.; Deserno, M. Aggregation and vesiculation of membrane proteins by curvature-mediated interactions. *Nature* **2007**, *447*, 461.
(37) Reynwar, B. J.; Deserno, M. Membrane composition-mediated protein-protein interactions. *Biointerphases* **2008**, *3*, FA117−FA124.
(38) Illya, G.; Deserno, M. Coarse-grained simulation studies of peptide-induced pore formation. *Biophys. J.* **2008**, *95*, 4163−4173.
(39) Cooke, I. R.; Deserno, M. Coupling between lipid shape and membrane curvature. *Biophys. J.* **2006**, *91*, 487−495.
(40) Pannuzzo, M.; McDargh, Z. A.; Deserno, M. The role of scaffold reshaping and disassembly in dynamin driven membrane fission. *eLife* **2018**, *7*, No. e39441.
(41) Hu, M.; Stanzione, F.; Sum, A. K.; Faller, R.; Deserno, M. Design principles for nanoparticles enveloped by a polymer-tethered lipid membrane. *ACS Nano* **2015**, *9*, 9942−9954.
(42) Vácha, R.; Martinez-Veracoechea, F. J.; Frenkel, D. Receptor-mediated endocytosis of nanoparticles of various shapes. *Nano Lett.* **2011**, *11*, 5391−5395.
(43) Zhang, L.; Chen, H.; Xie, J.; Wang, X. Interplay of Nanoparticle Rigidity and Its Translocation Ability through Cell Membrane. *J. Phys. Chem. B* **2019**, *123*, 8923.
(44) Humphrey, W.; Dalke, A.; Schulten, K. VMD − Visual Molecular Dynamics. *J. Mol. Graphics* **1996**, *14*, 33−38.
(45) Farago, O. "Water-free" computer model for fluid bilayer membranes. *J. Chem. Phys.* **2003**, *119*, 596−605.
(46) Tolpekina, T. V.; den Otter, W. K.; Briels, W. J. Simulations of stable pores in membranes: system size dependence and line tension. *J. Chem. Phys.* **2004**, *121*, 8014−8020.
(47) Weik, F.; Weeber, R.; Szuttor, K.; Breitsprecher, K.; de Graaf, J.; Kuron, M.; Landsgesell, J.; Menke, H.; Sean, D.; Holm, C. ESPResSo 4.0−an extensible software package for simulating soft matter systems. *Eur. Phys. J.: Spec. Top.* **2019**, *227*, 1789−1816.
(48) Kolb, A.; Dünweg, B. Optimized constant pressure stochastic dynamics. *J. Chem. Phys.* **1999**, *111*, 4453−4459.
(49) Macháň, R.; Hof, M. Lipid diffusion in planar membranes investigated by fluorescence correlation spectroscopy. *Biochim. Biophys. Acta, Biomembr.* **2010**, *1798*, 1377−1391.
(50) Terzi, M. M.; Deserno, M. *The Role of Mechanics in the Study of Lipid Bilayers*; Springer: 2018; pp 105−166, DOI: 10.1007/978-3-319-56348-0_3.
(51) Deserno, M. Fluid lipid membranes: From differential geometry to curvature stresses. *Chem. Phys. Lipids* **2015**, *185*, 11−45.
(52) Venable, R. M.; Brown, F. L.; Pastor, R. W. Mechanical properties of lipid bilayers from molecular dynamics simulation. *Chem. Phys. Lipids* **2015**, *192*, 60−74.
(53) Rawicz, W.; Olbrich, K. C.; McIntosh, T.; Needham, D.; Evans, E. Effect of chain length and unsaturation on elasticity of lipid bilayers. *Biophys. J.* **2000**, *79*, 328−339.
(54) Terzi, M. M.; Deserno, M. Novel tilt-curvature coupling in lipid membranes. *J. Chem. Phys.* **2017**, *147*, 084702.

https://dx.doi.org/10.1021/acs.jctc.0c00862
J. Chem. Theory Comput. 2020, 16, 7195−7206

(55) Terzi, M. M.; Ergüder, M. F.; Deserno, M. A consistent quadratic curvature-tilt theory for fluid lipid membranes. *J. Chem. Phys.* **2019**, *151*, 164108.
(56) Jablin, M. S.; Akabori, K.; Nagle, J. Experimental support for tilt-dependent theory of biomembrane mechanics. *Phys. Rev. Lett.* **2014**, *113*, 248102.
(57) Nagle, J. F. Experimentally determined tilt and bending moduli of single-component lipid bilayers. *Chem. Phys. Lipids* **2017**, *205*, 18−24.
(58) Safran, S. *Statistical thermodynamics of surfaces, interfaces, and membranes*; CRC Press: 2018.
(59) Rowlinson, J. S.; Widom, B. *Molecular theory of capillarity*; Courier Corporation: 2013.
(60) Irving, J.; Kirkwood, J. G. The statistical mechanical theory of transport processes. IV. The equations of hydrodynamics. *J. Chem. Phys.* **1950**, *18*, 817−829.
(61) Hardy, R. J. Formulas for determining local properties in molecular-dynamics simulations: Shock waves. *J. Chem. Phys.* **1982**, *76*, 622−628.
(62) Flyvbjerg, H.; Petersen, H. G. Error estimates on averages of correlated data. *J. Chem. Phys.* **1989**, *91*, 461−466.
(63) Terzi, M. M.; Deserno, M.; Nagle, J. F. Mechanical properties of lipid bilayers: a note on the Poisson ratio. *Soft Matter* **2019**, *15*, 9085−9092.
(64) Helfrich, W. In *Physics of Defects*; Balian, M., Kléman, R., Poirier, J. P., Eds.; North Holland: Amsterdam, 1981.
(65) Helfrich, W. Lyotropic Lamellar Phases. *J. Phys.: Condens. Matter* **1994**, *6*, A79−A92.
(66) Hamm, M.; Kozlov, M. Elastic energy of tilt and bending of fluid membranes. *Eur. Phys. J. E: Soft Matter Biol. Phys.* **2000**, *3*, 323−335.
(67) Doktorova, M.; LeVine, M. V.; Khelashvili, G.; Weinstein, H. A new computational method for membrane compressibility: Bilayer mechanical thickness revisited. *Biophys. J.* **2019**, *116*, 487−502.
(68) Marrink, S. J.; Risselada, H. J.; Yefimov, S.; Tieleman, D. P.; De Vries, A. H. The MARTINI force field: coarse grained model for biomolecular simulations. *J. Phys. Chem. B* **2007**, *111*, 7812−7824.

https://dx.doi.org/10.1021/acs.jctc.0c00862
J. Chem. Theory Comput. 2020, 16, 7195−7206